Atomic scale understanding of the permeation of plasma species across native and oxidized membranes

Atomic scale understanding of the permeation of plasma species across native and oxidized membranes

J. Razzokov[1],* M. Yusupov[1], R. M. Cordeiro[2] and A. Bogaerts[1]

[1] Research Group PLASMANT, Department of Chemistry, University of Antwerp, Universiteitsplein 1, B-2610 Antwerp, Belgium
[2] Centro de Ciências Naturais e Humanas, Universidade Federal do ABC, Avenida dos Estados 5001, CEP 09210-580, Santo André, SP, Brazil

E-mail: jamoliddin.razzokov@uantwerpen.be

Abstract

Cold atmospheric plasmas (CAPs) have attracted significant interest for their potential benefits in medical applications, including cancer therapy. The therapeutic effects of CAPs are related to reactive oxygen and nitrogen species (ROS and RNS) present in the plasma. The impact of ROS has been extensively studied, but the role of RNS in CAP-treatment remains poorly understood at the molecular level. Here, we investigate the permeation of RNS and ROS across native and oxidized phospholipid bilayers (PLBs) by means of computer simulations. The results reveal significantly lower free energy barriers for RNS (i.e., NO, NO_2, N_2O_4) and O_3 compared to hydrophilic ROS, such as OH, HO_2 and H_2O_2. This suggests that the investigated RNS and O_3 can permeate more easily through both native and oxidized PLBs in comparison to hydrophilic ROS, indicating their potentially important role in plasma medicine.

keywords

cold atmospheric plasma, reactive oxygen and nitrogen species, cell membrane, molecular dynamics, free energy profile

1. Introduction

Cold atmospheric plasmas (CAPs) are gaining increasing interest in many applications, such as bacterial decontamination, wound healing [1, 2], blood coagulation [3], as well as cancer treatment [4-6]. Specifically, CAPs show great potential in selective treatment of many cancer cell types, leaving normal cells less damaged [7, 8]. This might give an advantage to CAP over traditional anti-cancer therapies. The underlying mechanisms, however, are still unclear and need more fundamental investigations.

The selectivity of CAP towards cancer cells is linked to the elevated level of intracellular reactive oxygen and nitrogen species (ROS and RNS or RONS) found in cancer cells compared to normal cells [8-10]. These species cause nitro-oxidative stress in the cell and may even lead to cell death [4, 8, 11-13]. However, the precise action of RONS to cells still remains unknown. CAP-generated RONS most probably interact with and permeate through the cell membrane, thereby affecting intracellular processes through modification of internal cellular components. Hence, the study of RONS permeation across the cell membrane is essential, in order to understand the selective effect of CAP.

In this respect, the role of ROS has been studied extensively both experimentally [4-18] and by computer simulations [19-24], but far less attention has been paid to the effect of RNS, especially in terms of modeling. Indeed, experiments evidenced a noticeable rise of intracellular ROS concentrations after CAP treatment in cancer cells [8, 14]. This may result in ROS induced regulation of intracellular signaling pathways, which can lead to cell growth inhibition and cell death [15, 16, 24]. In recent reviews, Bauer showed the effect of

extracellular ROS in apoptosis-inducing signaling, and in particular the role of ROS in the inactivation of antioxidant proteins (e.g., catalase), which subsequently leads to tumor cell death [17, 18]. Interestingly, in his recent investigation, Bauer demonstrated that an increase of endogenous NO concentration causes catalase inactivation and reactivation of intercellular apoptosis signaling, specifically in tumor cells [13, 25]. The role of NO in blocking the electron transport chain in mitochondria was also reviewed [26]. It was indicated that NO acts through neutralizing cytochrome C oxidase, thereby resulting in an increase of the intracellular ROS level followed by triggering mitochondrial apoptosis [26]. Inactivation of the glutathione peroxidase by NO and its role in inducing apoptotic cell death was also reported [27]. Moreover, the combined action of NO with H_2O_2 to cause DNA damage, ultimately leading to programmed cell destruction, was evidenced in [28]. In addition, the role of peroxynitrite, which is generated by reaction of NO with superoxide in the cell, was studied in [29-33]. It was demonstrated that peroxynitrite inactivates catalase [29], manganese-superoxide dismutase [30], peroxiredoxin [31], glutathione peroxidase [32] and glutathione reductase [33], which overall deteriorates the antioxidant system of the cell. Thus, it appears that the cell becomes more vulnerable to the plasma generated exogenous RONS, due to the impairment of its antioxidant defense system. This in turn leads to further increase of intracellular reactive species [34, 35], causing nitro-oxidative stress in cells.

All the above mentioned studies indicate that the effect of CAP-generated RNS is also important to investigate, as RNS can play an essential role in apoptosis signaling pathways in cancer cells [11, 13, 25]. Studying the role of RNS (together with the role of ROS) helps to reveal a more complete picture of the selective effect of CAP on cancer cells, since CAP-generated RNS and ROS simultaneously act on the cancer cells, thereby inducing nitrosative and oxidative stress in these cells.

As mentioned above, the role of ROS was widely studied both by simulations and experiments in the context of plasma medicine. Computationally, we investigated ROS-induced oxidation of the phospholipid bilayer (PLB) and its subsequent effect on the PLB permeability [19-23]. Specifically, we studied the effect of CAP-induced lipid peroxidation on phosphatidylserine flip-flop across the PLB, which is involved in apoptotic signaling [19], as well as the formation of water pores induced by CAP-oxidation of PLB lipids [20], ROS oxidation of the headgroups and lipid tails in the cell membrane [21], the transport of ROS across oxidized and non-oxidized PLBs [36], including the synergistic effect of CAP oxidation and electric field [22], and the hampering effect of cholesterol [23].

As explained above, RNS also play an imperative role in CAP treatment of cancer cells [13, 25, 37]. Although the effects of selected ROS have been widely studied, far less attention has been paid to RNS. Hence, in this paper, we investigate the permeation of ROS and RNS across native and oxidized PLBs. The reason for studying oxidized membranes, besides native PLBs, is that CAP can cause lipid oxidation in the cell membrane [21], and the effect of this oxidation on the transmembrane transport of ROS and RNS should also be studied, and compared with the behavior for non-oxidized (native) PLBs.

Thus, in the present study, we calculate the free energy profiles (FEPs) of RNS (NO, NO_2, N_2O_4) across native and oxidized PLBs, and we compare them with calculated FEPs for ROS (O_2, O_3, OH, HO_2, and H_2O_2).

2. Simulation setup

We performed molecular dynamics (MD) simulations to study the transport of the aforementioned species (i.e., OH, HO_2, H_2O_2, O_3, NO, NO_2, N_2O_4) through native and oxidized membranes. As a model system we considered the PLB representing the cell membrane. Each PLB included 128 phospholipids (PLs), equally distributed in both layers of

the membrane, together with 8000 water molecules surrounding them (see Fig. 1a). We considered a native PLB made of 1,2-dioleoyl-*sn*-glycero-3-phosphocholine (DOPC) and an oxidized PLB made of a 1:1 homogeneous mixture of DOPC and its aldehyde oxidation product (DOPC-ALD) (see Fig. 1b). We chose these PLs because (*i*) DOPC is one of the main components of the plasma membrane in both the outer and inner leaflet [38], and (*ii*) the aldehydes are one of the most commonly observed oxidation products [39]. Indeed, the mass spectrometry analysis in our previous study showed that the formation of aldehyde groups (i.e., DOPC-ALD) was prominently observed in CAP-treated vesicles [21]. Note that the cell membrane itself consists of different types of membrane components, including phospholipids, proteins, sterols, etc. Practically, due to the computational cost, we cannot mimic in our simulations the real membrane composition, because even the simplest plasma membrane of a red blood cell consists of over 150 lipid species. Hence, we should focus on the main lipid components and therefore, in our model system we chose DOPC as a primary element of a PLB. This type of lipid molecules is found e.g., in 40, 44% and 24% of the endoplasmic reticulum, mitochondrion membrane and liver cell plasma membrane, respectively [40].

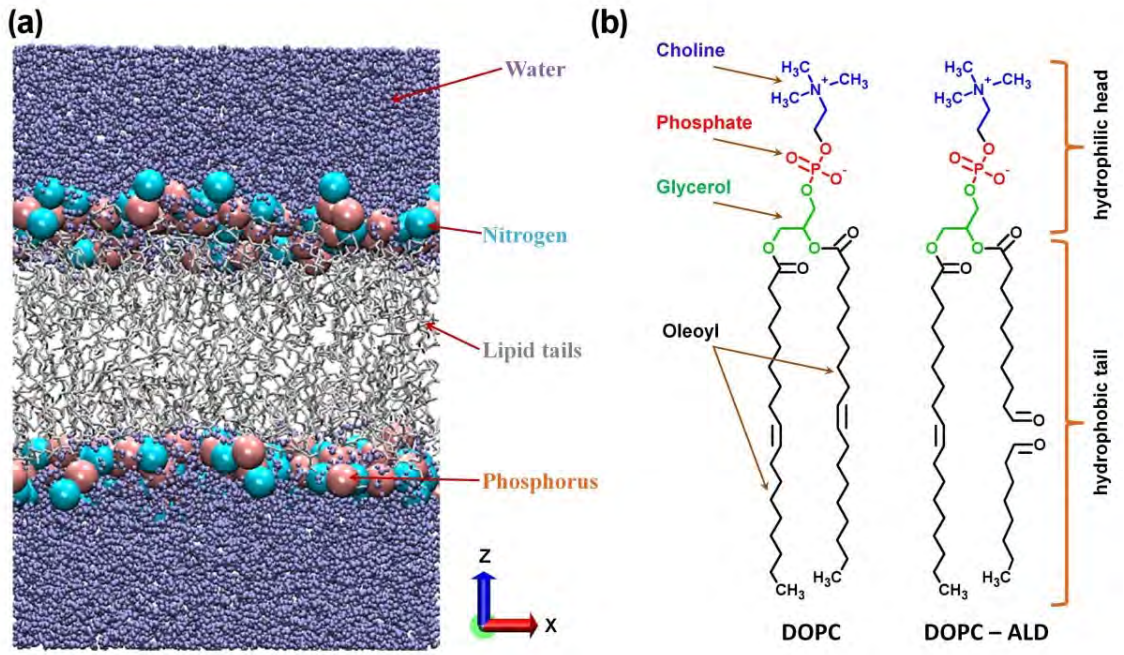

Figure 1. (a) Native DOPC PLB. The P and N atoms are shown with larger beads for the sake of clarity. (b) Schematic representation of native (DOPC) and oxidized (DOPC-ALD) PLs.

The presence of 50% DOPC-ALD in the oxidized PLB was high enough to observe the effect of oxidation, but low enough so that pore formation did not occur within the simulated time scale [20]. The initial configurations of the native and oxidized PLBs were created by means of the Packmol package [41]. All simulations were performed employing the GROMACS-5.1 package [42]. We used the GROMOS (43A1-S3) united atom force field for native phospholipids [43], supplemented with additional parameters for the aldehyde derivative [43]. GROMOS-type force field parameters for ROS and RNS were obtained from [36, 44]. These parameters were chosen because they have been demonstrated to yield correct water-to-alkane partition coefficients of ROS and RNS, which are essential for the proper description of transmembrane permeation. These parameters were supplemented with our own NO force

field, which was derived following the same protocols as in [36] and [44] (see Appendix for further details).

The model membranes were initially energy minimized with the steepest descent algorithm and then equilibrated for 200 ns in the isothermal-isobaric (NPT) ensemble at 1 bar and 310 K. The equilibration runs were performed employing the semi-isotropic Parrinello-Rahman barostat with compressibility and coupling constant of 4.5×10^{-5} bar^{-1} and 0.1 ps, respectively, as well as the Nose-Hoover thermostat with a coupling constant of 0.2 ps. The particle mesh Ewald (PME) method was used to treat electrostatic interactions with a real space cut-off of 1.0 nm, in combination with a 0.15 nm spaced-grid for the reciprocal-space interactions. All simulations were carried out using a time step of 2 fs, and periodic boundary conditions were applied in all three directions.

To calculate the FEPs associated to the transmembrane translocation of ROS and RNS, we applied the umbrella sampling (US) method [45, 46].

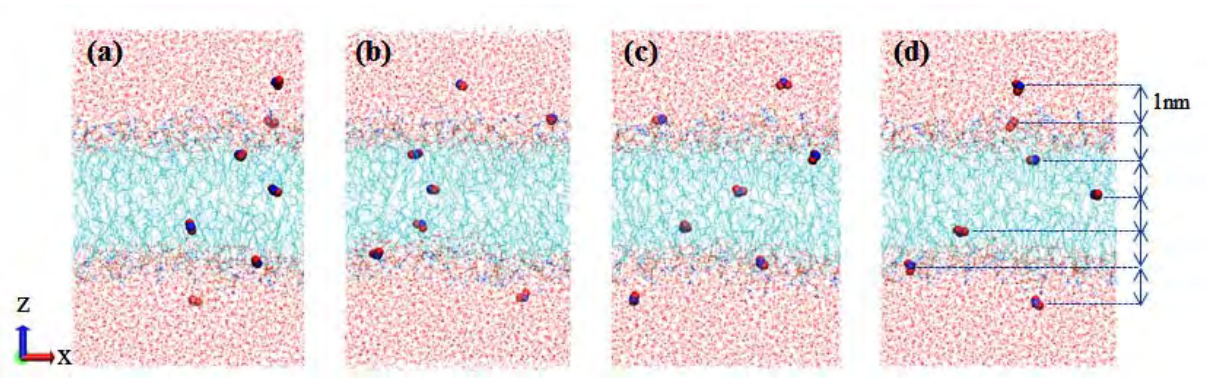

Figure 2. Four model systems of native DOPC PLB. The model systems are derived from 170 ns (a), 180 ns (b), 190 ns (c) and 200 ns (d) of equilibration run trajectories. In this example, seven NO_2 species are inserted in each model system, randomly in the xy plane, but separated by 1 nm distance in the z-direction.

Initial membrane structures for the US simulations were selected from the last 30 ns of equilibration. In order to save computational resources, US simulations were performed as follows. Four membrane structures were selected from the last 30 ns of equilibration. In each of the US simulations, 7 permeants were distributed along the membrane normal, keeping a distance of 1 nm between each other (Fig. 2). To keep the permeants at their positions with respect to the membrane center, their center-of-mass motion was restricted along the *z*-axis by harmonic biases with force constants of 2000 $kJ\cdot mol^{-1}\cdot nm^{-2}$. At the *xy*-plane, the permeants were still free to move. A US simulation was performed at NPT for each system, comprising 2 ns of equilibration and 4 ns of sampling. The umbrella histograms were collected and an individual FEP was built by the weighted histogram analysis method (WHAM) [47]. We performed 10 US simulations (6 ns each) to build one individual FEP; thus, for each FEP 7x10=70 US windows are defined along the membrane normal, which are separated by 1 Å. For every combination of permeant (i.e., OH, HO_2, H_2O_2, O_3, NO, NO_2, N_2O_4) and PLB (DOPC, DOPC-ALD), i.e., 14 combinations in total, we calculated between 16 and 24 individual FEPs, which were then averaged. Thus, in total we performed between 0.96 and 1.44 μs of US for each permeant in both DOPC and DOPC-ALD. 1 μs of US simulation takes about 42 days in real computing time. Note that the data collected for the calculation of FEPs strongly depend on the lipid composition surrounding the randomly placed RONS in the PLB. To estimate a true free energy barrier, good statistics is necessary. Moreover, the comparison of the symmetric and full (i.e., asymmetric) FEPs for each RONS is needed to verify the data convergence of the simulations. We obtained very symmetric FEPs, which are a hallmark for convergence of the simulations (see Figure A1 in Appendix).

It should be mentioned that in reality, chemical reactions of RONS might take place in the PLB. However, these processes cannot be revealed by performing conventional non-reactive MD simulations, due to the limitations of the used potential. Nevertheless, the electronic degrees of freedom needed to describe chemical reactions are not explicitly considered in classical MD. Even so, the US simulations help to determine the RONS permeation rate across the PLB before and after oxidation, through calculations of the FEPs. Besides, the most probable accumulation regions for RONS also can be predicted based on the FEPs that give a possibility to study position-dependent specific interactions in the membrane with possible implications for reactivity.

3. Results and discussion

Figure 3 shows the FEPs of various ROS and RNS across native and oxidized PLBs. As the hydrophilic ROS (OH, HO_2, H_2O_2) are moved from the aqueous phase to the membrane interior, the FEP first decreases, reaching a minimum at the headgroup region, and then increases as ROS are placed deeper into the native PLB (Fig. 3a). In all cases, the free energy barrier is located at the PLB core. Adsorption at the headgroup region is much stronger for H_2O_2 and HO_2, and H_2O_2 has the largest permeation barrier among all hydrophilic ROS. In an earlier study, we identified specific ROS-membrane interactions that may be responsible for these trends [36]. It was proposed that ROS adsorption at the PLB surface is mainly driven by two factors: (*i*) H-bond interactions between ROS and the PL carbonyl ester groups, and (*ii*) dispersion interactions with the headgroup region. Although all the hydrophilic ROS investigated are H-bond donors, H_2O_2 and HO_2 have an extra O atom that leads to stronger dispersion interactions in comparison to the smaller OH radical. That might explain the differences in the adsorption tendencies of the hydrophilic ROS. Besides that, H_2O_2 is known for its ability to establish twice as many H-bonds in water, as compared to OH and HO_2 [36]. That might explain the largest permeation barrier recorded for H_2O_2. When the PLB is oxidized, the permeation follows similar qualitative trends, but with smaller free energy barriers (Fig. 3b). PL oxidation generates functional groups and fragments that increase the hydrophilicity of the membrane core, leading to an increase of the PLB permeability to ROS [22]. Although the permeation barrier still remains relatively high for H_2O_2, it becomes significantly lower for OH. Most notably, in the case of HO_2, PLB oxidation apparently even leads to a change of its partition behavior. The FEPs suggest that HO_2 might develop a preference for the PLB core as oxidation takes place. This effect is especially important because HO_2 is the protonated form of the biologically relevant superoxide radical (O_2^-). However, we also note that this result is still speculative. The HO_2 model has originally been parametrized to reproduce its experimentally measured hydration free energy [36]. Hydrophobic solvation has not been considered, as there was no reference experimental data available. To draw more conclusive data, one would need to evaluate the performance of the HO_2 model in the description of its solvation free energy in non-polar solvents.

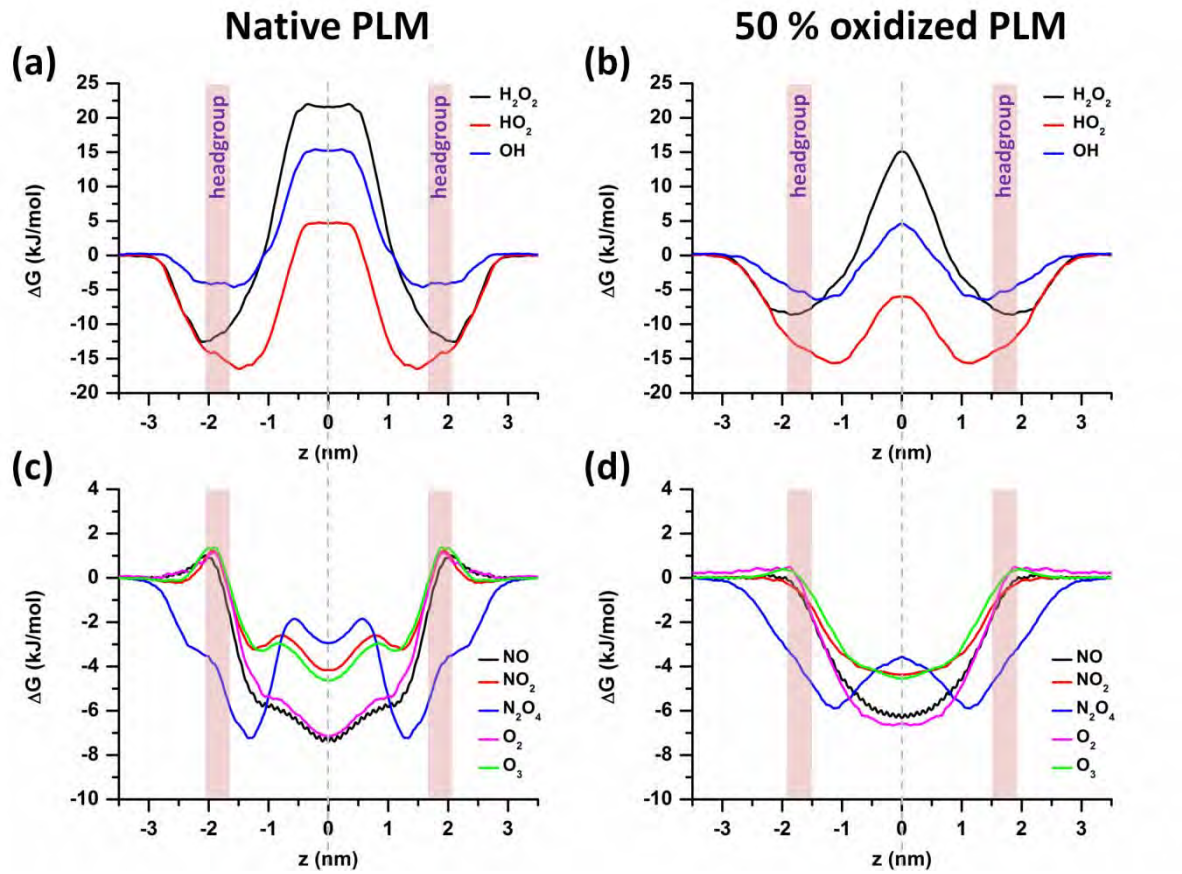

Figure 3. FEPs of the hydrophilic (a-b) and hydrophobic (c-d) ROS and RNS, across the native and 50% oxidized PLBs. The average positions of the headgroup regions (i.e., average position of phosphate atoms, cf. Fig. 1) are indicated by light red color.

The hydrophobic species show a completely different behavior (see Fig. 3c,d; and note the different scale of the y-axis). In the native PLB, NO, NO_2, O_2 and O_3 exhibit very low permeation barriers, which are all located at the headgroup region (Fig. 3c). The free energy at the PLB core is lower than in the aqueous phase, indicating that these species have a tendency to partition to the PLB interior. The FEPs suggest that O_2 and NO, which are practically non-polar, have the strongest tendency to accumulate in the PLB interior, followed by the triatomic species NO_2 and O_3, which still conserve a residual dipole moment [44]. N_2O_4 differentiates from the other species, as it experiences no energy barrier at the headgroup region, but in contrast, a free energy minimum is found close to this region. By moving deeper toward the PLB center, the free energy increases, but reaches values that are closer to the free energy in bulk water. The barrier around the center of the PLB (i.e., at ~ |0.7| nm) is due to the double bond of the oleoyl tails, which results in bending of the lipid chains. This barrier is also slightly visible for the other hydrophobic species (cf. NO_2 and O_3 in Fig. 3c). The results suggest that N_2O_4 has affinity for the membrane surface, but partitions almost equally between the aqueous phase and the PLB core. The FEP of N_2O_4 has hybrid characteristics of hydrophilic and hydrophobic species. The geometry of N_2O_4 is such that it has no dipole moment, but the partial charges that develop at the N and O atoms are relatively large (+0.584*e* and -0.292*e*, respectively) [44]. It might conceivably lead to a strong quadrupole moment, which might explain the tendency of N_2O_4 to accumulate near to the headgroup region, where it is not as hydrated as in the aqueous phase, but still interacts with the polar PL headgroups. PLB oxidation does not cause significant changes to the permeation

of hydrophobic ROS and RNS, except that the FEPs are smoother (Fig. 3d). Indeed, the local free energy barriers at ~ |0.7| nm are gone (cf. Fig. 3c and 3d). This is due to the cleavage of the lipid tails and the formation of aldehyde groups (cf. Fig. 1b and see Fig. 3d). The removal of the local free energy barriers is because of the membrane fluidity: the surface area of the PLB increases and the membrane thickness decreases due to disordering in the lipid tails [22]. Nevertheless, the accumulation position is still in the center of the PLB for hydrophobic species, except for N_2O_4.

Taken together, our simulation results agree with previously reported experimental measurements of PLB permeability. Indeed, the permeability of hydrophobic species, like NO and O_2, was found to be 3-6 orders of magnitude higher than the permeability of hydrophilic ROS, like H_2O_2 [48, 49]. Therefore, membrane-embedded aquaporin channels, or pores created by e.g., strong electric fields [22], are required to improve the transport of hydrophilic ROS in and out of the cell. Indeed, we recently found that the permeability of H_2O_2 through AQP is two orders of magnitude higher than through the PLB [50]. In the case of hydrophobic ROS and RNS, transmembrane transport may easily take place even in the absence of channels and pores. This was also demonstrated in literature, where a higher permeability coefficient was reported [51], e.g., 18-93 cm/s for NO [49, 52, 53], 5 cm/s for NO_2 [53] and 12-157 cm/s for O_2 [49, 52, 54-56], whereas for H_2O_2 it varies between $4x10^{-4}$ and $1.2x10^{-2}$ cm/s [51]. Although all RNS investigated here are hydrophobic, we note that hydrophilic RNS, such as HNO_2, HNO_3/NO_3^- and peroxynitrous acid (ONOOH), can also be generated by plasma processes. However, we could not include these species in the present study, as the force field used in the simulations to describe the behavior of these species is not available yet and therefore we could not yet study their behavior. Future studies will reveal how these hydrophilic RNS interact with native and oxidized PLBs.

As mentioned above, the cell membrane by nature is a complex system and contains different types of membrane components. Consequently, these components might also influence the permeation of RONS into the cytoplasm. It is clear that we cannot study the effect of all these components. In our previous investigation we studied the effect of cholesterol on the FEPs of ROS (i.e., OH, HO_2, H_2O_2 and O_2) [23]. We found that the presence of cholesterol increases the lipid order, thereby increasing the free energy barrier for ROS penetration. Hence, we may conclude that the inclusion of cholesterol to our model system might affect the FEPs of the studied RONS, by increasing their free energy barriers. However, we expect that this might eventually lead to the same trends in the FEPs, and thus to the same qualitative conclusions.

4. Conclusions

In general, we can conclude that hydrophobic species, like NO, NO_2, N_2O_4, O_2 and O_3, can significantly better penetrate across both native and oxidized PLBs, compared to hydrophilic ROS, such as OH, HO_2 and H_2O_2, due to the considerably lower free energy barriers.

Oxidation of the PLB caused by e.g., CAP does not strongly affect the free energy barriers of NO, NO_2, N_2O_4, O_2 and O_3, whereas it reduces the barriers of OH, HO_2 and H_2O_2, thereby increasing their translocation probability across the oxidized PLB.

This study is essential for plasma medicine and it is one step towards the understanding of the penetration capabilities of different RONS (generated by CAP) through the native and oxidized cell membrane. Further detailed investigations are needed in order to gain insight into the cooperative role of these species in intracellular signaling processes.

Note that the unique feature of CAP is that it generates a cocktail of various reactive species, ions, UV as well as electric field. Obviously, all these phenomena cannot be captured by our non-reactive MD simulations. Some of them, e.g., the reactions of RONS with the cell

membrane components, can be studied using very accurate computational tools, i.e., quantum mechanical (QM) calculations. However, these methods also have limitations, i.e., they operate at standard system sizes in the order of 100 atoms and time scales of picoseconds. This might be overcome by a combination of QM calculations with molecular mechanics (MM, i.e., non-reactive MD simulations), which is called QM/MM method. This method will be investigated in our future studies.

Acknowledgements
M.Y. gratefully acknowledges financial support from the Research Foundation – Flanders (FWO), grant 1200216N. The computational work was carried out using the Turing HPC infrastructure at the CalcUA core facility of the Universiteit Antwerpen (UA), a division of the Flemish Supercomputer Center VSC, funded by the Hercules Foundation, the Flemish Government (department EWI) and the UA. R.M.C. thanks FAPESP and CNPq for financial support (grants 2012/50680-5 and 459270/2014-1, respectively).

Appendix

NO parametrization

Lennard-Jones interaction parameters were taken from atom types OO [36] and NQ [44]. A bond length of 0.1151 nm was considered [57]. These parameters led to the correct solvation free energy in cyclohexane. Partial charges were initially estimated by electronic structure calculations using the Gaussian 09 software [58]. Calculations were based on density functional theory with the B3LYP functional, the 6-311+G(3df,2pd) basis set and the ChelpG charge fitting scheme. Partial charges were then iteratively scaled to account for solvent-induced polarization effects and yield the correct hydration free energy. Solvation free energies were calculated by the thermodynamic integration method using 21 points for van der Waals and 11 points for Coulomb interactions. Production runs according to the NPT ensemble were performed for 1 ns. Further details about the simulation conditions were the same as in [36] and [44]. In the end, partial charges of +0.02*e* and -0.02*e* were found for the O and N atoms, respectively. Table A1 shows the solvation data for our newly derived NO model, as compared to a previous NO force field [59] and to experimental data [60, 61]. The results demonstrate that our NO model correctly describes both the aqueous and the hydrophobic solvation of NO, and is therefore suitable for studies of water/membrane partition of this species.

Table A1. *Solvation free energies of NO in cyclohexane and water, and the resulting partition coefficients (K).*

Force field	ΔG_{ch} **(kJ/mol)**	ΔG_{w} **(kJ/mol)**	$\Delta G_{w\rightarrow ch}$ **(kJ/mol)**	$K_{w\rightarrow ch}$
Victor *et al.*	-4.0	7.5	-11.5	103.7
this work	2.5	7.0	-4.5	6.1
experimental	2.1	7.6	-5.5	9.2

Comparison of full (i.e., non-symmetrized) and symmetrized FEPs

The obtained FEPs from the US simulations for RONS were perfectly converged. As an example, we show in Fig. A1 the full (i.e., non-symmetrized) and symmetrized FEPs of NO, NO_2, N_2O_4 and O_3 for native and 50% oxidized PLBs. As is clear, the full and symmetrized

FEPs are almost the same. Overlapping of the full and symmetrized FEPs is a hallmark of convergence of our data.

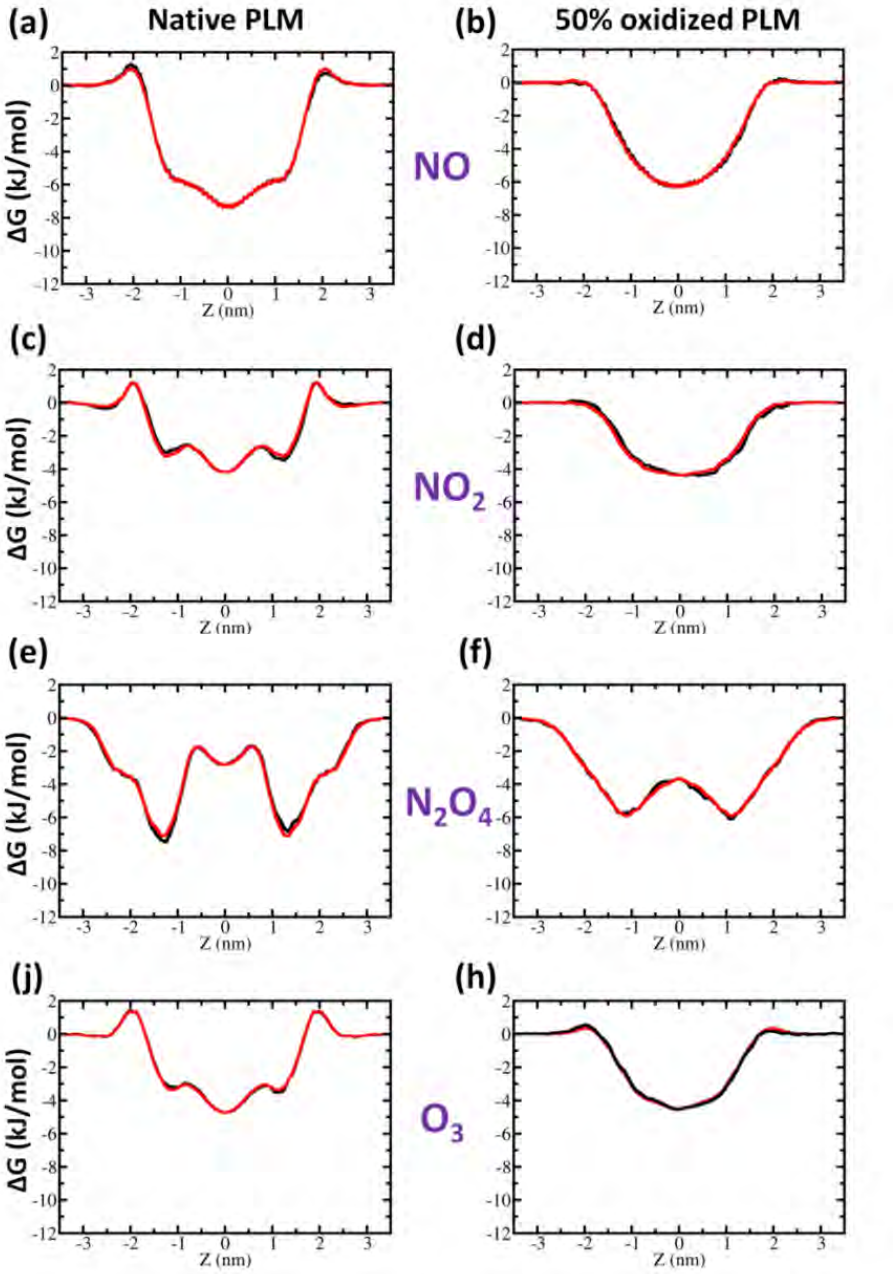

Figure A1. *Illustration of the full (— black line) and symmetrized (— red line) free energy profiles of NO (a-b), NO_2 (c-d), N_2O_4 (e-f) and O_3 (j-h) for native and 50% oxidized PLB.*

References

[1] Bekeschus S, Schmidt A, Weltmann K-D and von Woedtke T 2016 The plasma jet kINPen–a powerful tool for wound healing *Clinical Plasma Medicine* **4** 19-28

[2] Haertel B, von Woedtke T, Weltmann K-D and Lindequist U 2014 Non-thermal atmospheric-pressure plasma possible application in wound healing *Biomolecules & therapeutics* **22** 477

[3] Kalghatgi S U, Fridman G, Cooper M, Nagaraj G, Peddinghaus M, Balasubramanian M, Vasilets V N, Gutsol A F, Fridman A and Friedman G 2007 Mechanism of blood coagulation by

nonthermal atmospheric pressure dielectric barrier discharge plasma *IEEE Transactions on plasma science* **35** 1559-66

[4] Keidar M, Walk R, Shashurin A, Srinivasan P, Sandler A, Dasgupta S, Ravi R, Guerrero-Preston R and Trink B 2011 Cold plasma selectivity and the possibility of a paradigm shift in cancer therapy *British journal of cancer* **105** 1295

[5] Barekzi N and Laroussi M 2012 Dose-dependent killing of leukemia cells by low-temperature plasma *Journal of Physics D: Applied Physics* **45** 422002

[6] Vermeylen S, De Waele J, Vanuytsel S, De Backer J, Van der Paal J, Ramakers M, Leyssens K, Marcq E, Van Audenaerde J and LJ Smits E 2016 Cold atmospheric plasma treatment of melanoma and glioblastoma cancer cells *Plasma Processes and Polymers* **13** 1195-205

[7] Iseki S, Nakamura K, Hayashi M, Tanaka H, Kondo H, Kajiyama H, Kano H, Kikkawa F and Hori M 2012 Selective killing of ovarian cancer cells through induction of apoptosis by nonequilibrium atmospheric pressure plasma *Applied Physics Letters* **100** 113702

[8] Kim S J and Chung T 2016 Cold atmospheric plasma jet-generated RONS and their selective effects on normal and carcinoma cells *Scientific reports* **6** 20332

[9] Liou G-Y and Storz P 2010 Reactive oxygen species in cancer *Free radical research* **44** 479-96

[10] Wiseman H and Halliwell B 1996 Damage to DNA by reactive oxygen and nitrogen species: role in inflammatory disease and progression to cancer *Biochemical Journal* **313** 17

[11] Graves D B 2014 Reactive species from cold atmospheric plasma: implications for cancer therapy *Plasma Processes and Polymers* **11** 1120-7

[12] Redza-Dutordoir M and Averill-Bates D A 2016 Activation of apoptosis signalling pathways by reactive oxygen species *Biochimica et Biophysica Acta (BBA)-Molecular Cell Research* **1863** 2977-92

[13] Bauer G 2015 Increasing the endogenous NO level causes catalase inactivation and reactivation of intercellular apoptosis signaling specifically in tumor cells *Redox biology* **6** 353-71

[14] Yan D, Sherman J H and Keidar M 2017 Cold atmospheric plasma, a novel promising anti-cancer treatment modality *Oncotarget* **8** 15977-95

[15] Tanaka H, Mizuno M, Ishikawa K, Nakamura K, Kajiyama H, Kano H, Kikkawa F and Hori M 2011 Plasma-activated medium selectively kills glioblastoma brain tumor cells by down-regulating a survival signaling molecule, AKT kinase *Plasma Medicine* **1**

[16] Ishaq M, Evans M M and Ostrikov K K 2014 Effect of atmospheric gas plasmas on cancer cell signaling *International journal of cancer* **134** 1517-28

[17] Bauer G 2012 Tumor cell-protective catalase as a novel target for rational therapeutic approaches based on specific intercellular ROS signaling *Anticancer research* **32** 2599-624

[18] Bauer G 2014 Targeting extracellular ROS signaling of tumor cells *Anticancer research* **34** 1467-82

[19] Razzokov J, Yusupov M, Vanuytsel S, Neyts E C and Bogaerts A 2017 Phosphatidylserine flip-flop induced by oxidation of the plasma membrane: a better insight by atomic scale modeling *Plasma Processes and Polymers* **14**

[20] Van der Paal J, Neyts E C, Verlackt C C and Bogaerts A 2016 Effect of lipid peroxidation on membrane permeability of cancer and normal cells subjected to oxidative stress *Chemical Science* **7** 489-98

[21] Yusupov M, Wende K, Kupsch S, Neyts E, Reuter S and Bogaerts A 2017 Effect of head group and lipid tail oxidation in the cell membrane revealed through integrated simulations and experiments *Scientific Reports* **7** 5761

[22] Yusupov M, Van der Paal J, Neyts E and Bogaerts A 2017 Synergistic effect of electric field and lipid oxidation on the permeability of cell membranes *Biochimica et Biophysica Acta (BBA)-General Subjects* **1861** 839-47

[23] Van der Paal J, Verheyen C, Neyts E C and Bogaerts A 2017 Hampering Effect of Cholesterol on the Permeation of Reactive Oxygen Species through Phospholipids Bilayer: Possible Explanation for Plasma Cancer Selectivity *Scientific reports* **7** 39526

[24] Yusupov M, Lackmann J W, Razzokov J, Kumar S, Stapelmann K and Bogaerts A 2018 Impact of plasma oxidation on structural features of human epidermal growth factor *Plasma Processes and Polymers* **15** e1800022
[25] Bauer G 2017 Nitric Oxide Contributes To Selective Apoptosis Induction In Malignant Cells Through Multiple Reaction Steps *Critical Reviews™ in Oncogenesis*
[26] Moncada S and Erusalimsky J D 2002 Does nitric oxide modulate mitochondrial energy generation and apoptosis? *Nature Reviews Molecular Cell Biology* **3** 214
[27] Asahi M, Fujii J, Suzuki K, Seo H G, Kuzuya T, Hori M, Tada M, Fujii S and Taniguchi N 1995 Inactivation of glutathione peroxidase by nitric oxide Implication for cytotoxicity *Journal of Biological Chemistry* **270** 21035-9
[28] Filep J G, Lapierre C, Lachance S and Chan J 1997 Nitric oxide co-operates with hydrogen peroxide in inducing DNA fragmentation and cell lysis in murine lymphoma cells *Biochemical Journal* **321** 897
[29] Keng T, Privalle C T, Gilkeson G S and Weinberg J B 2000 Peroxynitrite formation and decreased catalase activity in autoimmune MRL-lpr/lpr mice *Molecular Medicine* **6** 779
[30] Surmeli N B, Litterman N K, Miller A-F and Groves J T 2010 Peroxynitrite mediates active site tyrosine nitration in manganese superoxide dismutase. Evidence of a role for the carbonate radical anion *Journal of the American Chemical Society* **132** 17174-85
[31] Peshenko I V and Shichi H 2001 Oxidation of active center cysteine of bovine 1-Cys peroxiredoxin to the cysteine sulfenic acid form by peroxide and peroxynitrite *Free Radical Biology and Medicine* **31** 292-303
[32] Padmaja S, Squadrito G L and Pryor W A 1998 Inactivation of glutathione peroxidase by peroxynitrite *Archives of biochemistry and biophysics* **349** 1-6
[33] Savvides S N, Scheiwein M, Böhme C C, Arteel G E, Karplus P A, Becker K and Schirmer R H 2002 Crystal structure of the antioxidant enzyme glutathione reductase inactivated by peroxynitrite *Journal of Biological Chemistry* **277** 2779-84
[34] Ja Kim S, Min Joh H and Chung T 2013 Production of intracellular reactive oxygen species and change of cell viability induced by atmospheric pressure plasma in normal and cancer cells *Applied Physics Letters* **103** 153705
[35] Yan D, Talbot A, Nourmohammadi N, Cheng X, Canady J, Sherman J and Keidar M 2015 Principles of using cold atmospheric plasma stimulated media for cancer treatment *Scientific reports* **5** 18339
[36] Cordeiro R M 2014 Reactive oxygen species at phospholipid bilayers: distribution, mobility and permeation *Biochimica et Biophysica Acta (BBA)-Biomembranes* **1838** 438-44
[37] Graves D B 2012 The emerging role of reactive oxygen and nitrogen species in redox biology and some implications for plasma applications to medicine and biology *Journal of Physics D: Applied Physics* **45** 263001
[38] Ingólfsson H I, Melo M N, Van Eerden F J, Arnarez C m, Lopez C A, Wassenaar T A, Periole X, De Vries A H, Tieleman D P and Marrink S J 2014 Lipid organization of the plasma membrane *Journal of the american chemical society* **136** 14554-9
[39] Reis A, Domingues M, Amado F M, Ferrer-Correia A and Domingues P 2005 Separation of peroxidation products of diacyl-phosphatidylcholines by reversed-phase liquid chromatography–mass spectrometry *Biomedical Chromatography* **19** 129-37
[40] Alberts B, Lewis J, Morgan D, Raff M, Roberts K and Walter P 2014 Molecular Biology of the Cell, *Garland Science*
[41] Martínez L, Andrade R, Birgin E G and Martínez J M 2009 PACKMOL: a package for building initial configurations for molecular dynamics simulations *Journal of computational chemistry* **30** 2157-64
[42] Van Der Spoel D, Lindahl E, Hess B, Groenhof G, Mark A E and Berendsen H J 2005 GROMACS: fast, flexible, and free *Journal of computational chemistry* **26** 1701-18
[43] Chiu S-W, Pandit S A, Scott H and Jakobsson E 2009 An improved united atom force field for simulation of mixed lipid bilayers *The Journal of Physical Chemistry B* **113** 2748-63

[44] Cordeiro R M 2018 Reactive oxygen and nitrogen species at phospholipid bilayers: Peroxynitrous acid and its homolysis products. Journal of Physical Chemistry B (https://doi.org/10.1021/acs.jpcb.8b07158)
[45] Torrie G M and Valleau J P 1977 Nonphysical sampling distributions in Monte Carlo free-energy estimation: Umbrella sampling *Journal of Computational Physics* **23** 187-99
[46] Kästner J 2011 Umbrella sampling *Wiley Interdisciplinary Reviews: Computational Molecular Science* **1** 932-42
[47] Kumar S, Rosenberg J M, Bouzida D, Swendsen R H and Kollman P A 1992 The weighted histogram analysis method for free-energy calculations on biomolecules. I. The method *Journal of computational chemistry* **13** 1011-21
[48] Möller M N, Li Q, Lancaster J R and Denicola A 2007 Acceleration of nitric oxide autoxidation and nitrosation by membranes *IUBMB life* **59** 243-8
[49] Subczynski W K, Lomnicka M and Hyde J S 1996 Permeability of nitric oxide through lipid bilayer membranes *Free radical research* **24** 343-9
[50] Yusupov M, Yan D, Cordeiro R M and Bogaerts A 2018 Atomic scale simulation of H2O2 permeation through aquaporin: toward the understanding of plasma cancer treatment *Journal of Physics D: Applied Physics* **51** 125401
[51] Möller M N, Lancaster Jr J R and Denicola A 2008 The interaction of reactive oxygen and nitrogen species with membranes *Current Topics in Membranes* **61** 23-42
[52] Denicola A, Souza J M, Radi R and Lissi E 1996 Nitric oxide diffusion in membranes determined by fluorescence quenching *Archives of biochemistry and biophysics* **328** 208-12
[53] Signorelli S, Möller M N, Coitiño E L and Denicola A 2011 Nitrogen dioxide solubility and permeation in lipid membranes *Archives of biochemistry and biophysics* **512** 190-6
[54] Subczynski W K, Hopwood L E and Hyde J S 1992 Is the mammalian cell plasma membrane a barrier to oxygen transport? *The Journal of general physiology* **100** 69-87
[55] Subczynski W K, Hyde J S and Kusumi A 1989 Oxygen permeability of phosphatidylcholine--cholesterol membranes *Proceedings of the National Academy of Sciences* **86** 4474-8
[56] Widomska J, Raguz M and Subczynski W K 2007 Oxygen permeability of the lipid bilayer membrane made of calf lens lipids *Biochimica et Biophysica Acta (BBA)-Biomembranes* **1768** 2635-45
[57] Haynes W M 2014 *CRC handbook of chemistry and physics*: CRC press)
[58] Frisch M, Trucks G, Schlegel H, Scuseria G, Robb M, Cheeseman J, Scalmani G, Barone V, Mennucci B and Petersson G 2009 Gaussian 09, Revision A. 1 [computer software] *Wallingford, CT, USA: Gaussian. Google Scholar*
[59] Victor B L, Baptista A M and Soares C M 2009 Dioxygen and nitric oxide pathways and affinity to the catalytic site of rubredoxin: oxygen oxidoreductase from Desulfovibrio gigas *JBIC Journal of Biological Inorganic Chemistry* **14** 853-62
[60] Young C L 1981 *Oxides of nitrogen* vol 8: Pergamon Press)
[61] Wilhelm E, Battino R and Wilcock R J 1977 Low-pressure solubility of gases in liquid water *Chemical reviews* **77** 219-62